RSC Advances

PAPER

View Article Online
View Journal | View Issue

Cite this: *RSC Adv.*, 2020, **10**, 8266

Aqueous aging of a silica coated TiO_2 UV filter used in sunscreens: investigations at the molecular scale with dynamic nuclear polarization NMR

Danielle L. Slomberg,[ab] Riccardo Catalano,[ab] Fabio Ziarelli,[c] Stéphane Viel,[de] Vincent Bartolomei,[ab] Jérôme Labille[ab] and Armand Masion*[ab]

Received 19th January 2020
Accepted 12th February 2020

DOI: 10.1039/d0ra00595a

rsc.li/rsc-advances

Short-term, aqueous aging of a commercial nanocomposite TiO_2 UV filter with a protective SiO_2 shell was examined in abiotic simulated fresh- and seawater. Under these conditions, the SiO_2 layer was quantitatively removed (~88–98%) within 96 hours, as determined using inductively coupled plasma-atomic emission spectroscopy (ICP-AES). While these bulk ICP-AES analyses suggested almost identical SiO_2 shell degradation after aging in fresh- and seawater, surface sensitive ^{29}Si dynamic nuclear polarization (DNP) solid-state nuclear magnetic resonance (SSNMR), with signal enhancements of 5–10× compared to standard SSNMR, was able to distinguish differences in the aged nanocomposites at the molecular level. DNP-SSNMR revealed that the attachment of the silica layer to the underlying TiO_2 core rested on substantial Si–O–Ti bond formation, bonds which were preserved after freshwater aging, yet barely present after aging in seawater. The removal of the protective SiO_2 layer is due to ionic strength accelerated dissolution, which could present significant consequences to aqueous environments when the photoactive TiO_2 core becomes exposed. This work demonstrates the importance of characterizing aged nanocomposites not only on the bulk scale, but also on the molecular level by employing surface sensitive techniques, such as DNP-NMR. Molecular level details on surface transformation and elemental speciation will be crucial for improving the environmental safety of nanocomposites.

Introduction

In July 2018, the Hawaiian government passed a bill, effective January 1, 2021, to ban the sale of over-the-counter sunscreens containing oxybenzone and/or octinoxate because of reported adverse effects on the marine environment, especially their potential to increase the bleaching of coral reefs.[1–7] As an alternative to oxybenzone and octinoxate (and organic UV absorbers in general), it is often advocated to use inorganic UV filters, such as zinc oxide (ZnO) and titanium dioxide (TiO_2). Inorganic UV filters are usually considered as less problematic with regard to human and environmental health while providing protection against UV damage that is equivalent to organic compounds.[8–11] Indeed, mineral filters have a better photostability compared to organic compounds that may degrade under UV radiation, forming potentially harmful radical species.[12,13] Also, permeation into (intact) skin is much less of a concern with mineral filters than with organic filters.[8–11] Nevertheless, claims of environmental sustainability, or at least benignness, associated with the use of inorganic UV filters may be overstated since ZnO and TiO_2 are known to be (phyto)toxic towards a number of organisms, *e.g.* ref. 14–17 including the coral reefs that they are supposed to help preserve.[18,19]

As a matter of fact, the apparent safety of mineral UV filters is intimately linked to the presence of coatings around the core of these particles. This is especially true for TiO_2, because of its marked photocatalytic properties, which contribute to most of the potential adverse effects of this material.[14,20] Aluminum- and silicon-based coatings have thus been used to protect human skin (and possibly environmental biota) against harmful photocatalytic effects. Furthermore, both the size of the TiO_2 core and its protective shell are being reduced from the micrometer to the nanometer range to provide superior UV reflection and absorption as well as improved aesthetics,[12] presenting a need to assess the human and environmental nanosafety of these composites as well.

The key to the environmental sustainability of TiO_2-based (both micro and nano) sunscreens rests primarily on the persistence and stability of the coating. In this context, both the mode and strength of attachment of the coating to the core material must be taken into consideration, in addition to the coating's resistance to aging/weathering. The main importance

[a]CNRS, Aix-Marseille Univ., IRD, INRA, Coll France, CEREGE, Europôle Arbois, BP 80, 13545 Aix en Provence, France. E-mail: masion@cerege.fr
[b]Labex SERENADE, Europôle Arbois, BP 80, 13545 Aix en Provence, France
[c]Aix-Marseille Univ., CNRS, Centrale Marseille, FSCM, 13397 Marseille, France
[d]Aix-Marseille Univ., CNRS, ICR, 13397 Marseille, France
[e]Institut Universitaire de France, 75231 Paris, France

in regarding the mode of attachment is to distinguish between weak attachment, which allows coating delamination (*i.e.* flaking-off due to mild chemical and/or mechanical stimuli), and strong attachment (*e.g.* extensive covalent bonding), which requires higher energy or aggressive/specific chemical interaction to be altered. In the case of strong attachment, the resistance of the coating to aging becomes the predominant factor, with the inherent resistance of the protective layer likely being modified by the presence of additional shell(s). Examining these surface processes requires the use of element specific probes to monitor the changes in speciation as the material ages. X-ray based techniques are largely used to determine the speciation of elements with $Z > 20$ and the use of synchrotron radiation provides the necessary sensitivity to observe surface phenomena. For elements with $Z < 20$, these techniques are difficult to implement or cannot be used at all. Nuclear Magnetic Resonance (NMR) on the other hand is an excellent speciation tool for light elements but is generally regarded as insufficiently sensitive. Nevertheless for nuclei with a good receptivity, NMR yields excellent results. As an example, in the case of a TiO_2 nanocomposite with successive Al (oxy)hydroxide and organic coatings, NMR showed that the external organic layer was rapidly lost upon aqueous aging, while the covalently bound AlOOH shell remained largely unaffected.[21] However, it has been reported that swimming pool chemicals caused enough degradation to the Al hydroxide layer to observe photocatalytic activity of the aged material.[22,23]

In the present paper, we investigated the abiotic aging of a commercial TiO_2–SiO_2 nanocomposite UV filter, *viz.* Eusolex® T-AVO, in simulated fresh- and seawater using bulk and molecular scale examinations of the material before and after the aging process, in an effort to contribute to a more comprehensive environment, health, and safety assessment. Bulk elemental analysis was performed to evaluate the stability of the SiO_2 shell surrounding the TiO_2 core. Dynamic nuclear polarization (DNP) solid-state nuclear magnetic resonance (SSNMR) was used to monitor the Si species present in the protective SiO_2 shell before and after aqueous aging. By using the DNP technique, sensitivity issues with traditional NMR experiments due to the low receptivity of ^{29}Si were circumvented.

Materials and methods

Commercial TiO_2 nanoparticle UV filter characterization

The commercially available Eusolex® T-AVO TiO_2 UV filter used in this study was obtained as a sample from Merck. This rutile TiO_2 UV filter is composed of a TiO_2 core, coated with a SiO_2 protective layer to prevent against TiO_2 photocatalytic effects. According to the manufacturer, the rod-shaped T-AVO UV filter is composed of 80% TiO_2 and 20% SiO_2, with a length of ~80 nm and width of ~30 nm (Ref. Merck Eusolex T technical data).

The pristine T-AVO composition was first characterized by inductively coupled plasma-atomic emission spectroscopy (ICP-AES). Specifically, 300 mg of the powder was heated stepwise to 920 °C, after which an alkaline fusion was performed to dissolve the residue for analysis of Ti (336.121 nm) and Si (251.611 nm) using a PerkinElmer 4300 DV ICP-AES.

The mineralogy of the T-AVO nanoparticles was confirmed with X-ray diffraction (XRD). Briefly, pristine T-AVO particles were deposited on a low-background silicon plate and analyzed with a PANalytical X0Pert PRO (Limeil-Brevannes, France) diffractometer equipped with Co Kα radiation (1.79 Å) at 40 kV and 40 mA. The sample was spun at 15 rpm and scanned with a 2θ range of 4–75°, step size of 0.033°, and time per step of 4.7 s.

To evaluate the size and morphology of the pristine T-AVO particles, as well as determine the thickness of the SiO_2 shell, an Ultra-high Resolution Hitachi SU 9000 scanning electron microscope (SEM) with energy dispersive X-ray spectroscopy (EDS) detection was used.

Aqueous solutions

The simulated freshwater used here was the commercially available, natural source, Cristaline® (Source de la Doye, Neyrolles, France), which has a pH of 7.5 and an ionic strength of ~5.8 mM. Artificial seawater was prepared by adding 29.5 g of Instant Ocean® salt to 1 L of ultrapure water and magnetically stirring to dissolve the salt. After 5 min, the agitation was stopped and the large grains of salt were allowed to sediment. The recovered supernatant, with a pH of 8.2 and an ionic strength of ~576 mM, was then used as the artificial seawater without further preparation. Complete details on the ionic composition of the simulated waters can be found in Table 1. Additionally, the effects of pH and ionic strength on the nanocomposite aging were evaluated using both ultrapure water (Merck-Millipore, Milli-Q® purification system, ≥18.2 MΩ cm, TOC ≤ 3 ppb, pH ~ 6) and a solution of 1 mM $NaHCO_3$ (pH 8).

Aging of T-AVO nanocomposite UV filters in aqueous solution

To evaluate the aging of the T-AVO particles under aqueous conditions, 2 mL of a 50 g L^{-1} T-AVO suspension freshly prepared in ultrapure water was injected into either 248 mL of freshwater (Cristaline®) or artificial seawater (Instant Ocean®) for a final T-AVO concentration of 400 mg L^{-1}. The suspensions were magnetically stirred (300 rpm) over 48 hours under both artificial daylight (HQI-BT lamp OSRAM, E40, 400 W) and in the dark. The temperature was monitored for all samples and remained constant at 23 °C. For the samples aged under artificial daylight, any evaporation was compensated for by adding the appropriate volume of ultrapure water after 6, 24, and 48 h of aging. After 48 h of aging, the agitation was stopped and the aged by-products were allowed to sediment for 48 h. These aged by-products were then separated from the supernatant, collected *via* centrifugation (1 h, 2675*g*), washed twice with absolute ethanol (1 h, 2675*g*), and dried for NMR spectroscopic analysis.

Degradation of the SiO_2 shell was also monitored by analyzing the concentration of Si species (<2 nm) released into the waters during the aging process. Briefly, following the 96 hours of aging, aliquots (10 mL) of the supernatant were recovered and centrifuged with Amicon® Ultra-15 10K centrifugal filter devices (10 000 MWCO, size retention limit

Table 1 Characteristics and composition of simulated fresh- and seawaters

	Freshwater (Cristaline®)[a], La Doye	Seawater Instant Ocean®[b]
pH	7.5	8.2
Ionic strength (mM)	5.8	576
Ca^{2+} (mM)	1.61	8.12
Mg^{2+} (mM)	0.14	44.94
Na^{+} (mM)	0.52	399.28
K^{+} (mM)	0.01	8.12
Bicarbonate (mM)	3.20	1.64
Cl^{-} (mM)	0.56	450.27
SO_4^{2-} (mM)	0.06	19.88
SiO_2 (mM)	0.03	0.014

[a] Composition des sources Cristaline, 2010, http://static.lequipier.com/media/24136-3044406.2.pdf. [b] M. J. Atkinson and C. Bingman, Elemental composition of commercial seasalts, *J. Aquaric. Aquat. Sci.*, 1997, **8**, 39–43.

$\sim$ 2 nm, Merck-Millipore) at 4000*g* for 1 h to separate any stable, aged T-AVO nanoparticles from the solution. The recovered filtrate was then analyzed for Si with ICP-AES (detection wavelength = 251.611 nm) as an indication of SiO_2 coating degradation from the T-AVO particles. The percentage of SiO_2 coating degradation was calculated by dividing the measured released Si concentration by the maximum possible Si content that could be released from the T-AVO SiO_2 shell (400 mg L^{-1} T-AVO composed of 7.85% Si = 31.4 mg L^{-1} Si).

NMR spectroscopic analysis of T-AVO protective SiO_2 layer

To provide insight as to the Si species present in the protective SiO_2 layer before and after aqueous aging, pristine and aged T-AVO nanocomposites were analyzed by ^{29}Si dynamic nuclear polarization (DNP) solid-state nuclear magnetic resonance (SSNMR).[24] These cross-polarization (CP) magic-angle spinning (MAS) experiments were recorded with a Bruker NMR Avance-III spectrometer (9.4 T) equipped with a 3.2 mm low-temperature MAS probe (Bruker Biospin, Wissembourg, France) and a gyrotron to provide the microwave (μw) irradiation of the sample (at 263.334 GHz) required for DNP. The samples were prepared according to the incipient wetness impregnation method[25] by wetting the nanocomposite (about 20 mg) with an aqueous solution of the DNP polarizing radical, AMUPol (15 mM, 30 μL).[26] Spectra were obtained at a temperature of 105 K with a MAS rate of 10 kHz. Other acquisition parameters were as follows: CP contact time, 4 ms; recycle delay, 4 s; number of scans, between 6k and 15k. In this study, the DNP technique was necessary due to the large gains in sensitivity it can bring about as compared to "standard" SSNMR (*i.e.* without DNP and at room temperature), thereby providing SSNMR spectra with a good signal-to-noise ratio that can be obtained within reasonable acquisition times. DNP signal enhancements ($\varepsilon_{Si,CP}$) between 5 and 10 were obtained. The pristine T-AVO sample was also analyzed by recording ^{29}Si single-pulse excitation (SPE) MAS experiments on a Bruker Avance 400 WB spectrometer operating at 79.5 MHz at the Spectropole facility (Aix-Marseille Univ., France). The main acquisition parameters were: MAS rate, 10 kHz; recycle delay, 20 s; and number of scans, 10k. For all NMR experiments, ^{29}Si chemical shifts were externally referenced with respect to tetramethylsilane. The MestReNova software was used for processing free induction decays and line fitting the spectra.

Results and discussion

Characterization of pristine T-AVO nanocomposite at bulk and molecular scale

Elemental analysis, XRD, and SEM-EDS were used to characterize the bulk pristine T-AVO nanocomposites. Indeed, TiO_2 and SiO_2 concentrations determined with ICP-AES (80.2 ± 3.2 wt% and 16.8 ± 0.1 wt%, respectively) confirmed the composition reported by the manufacturer. As shown in Fig. 1, XRD analysis validated the rutile composition of the TiO_2 core. However, no silica presence was observed with XRD despite the SiO_2 representing ~17 wt% of the nanocomposite. Scanning electron microscopy (Fig. 2A) revealed a size range of 15–20 × 30–80 nm for the T-AVO nanocomposite, while the elemental map (Ti and

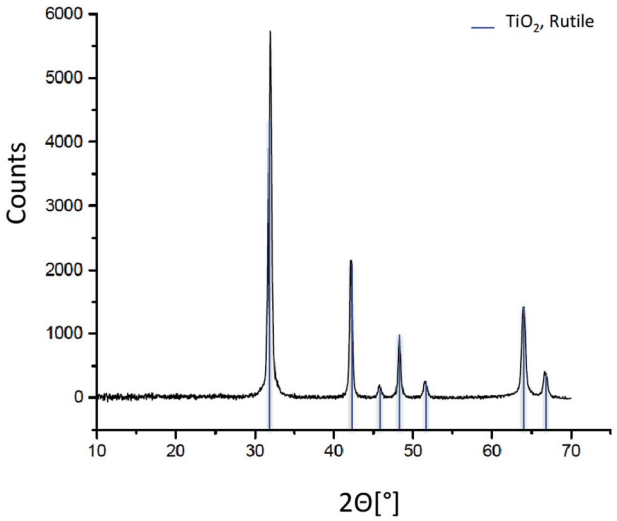

Fig. 1 X-ray diffraction pattern of pristine T-AVO.

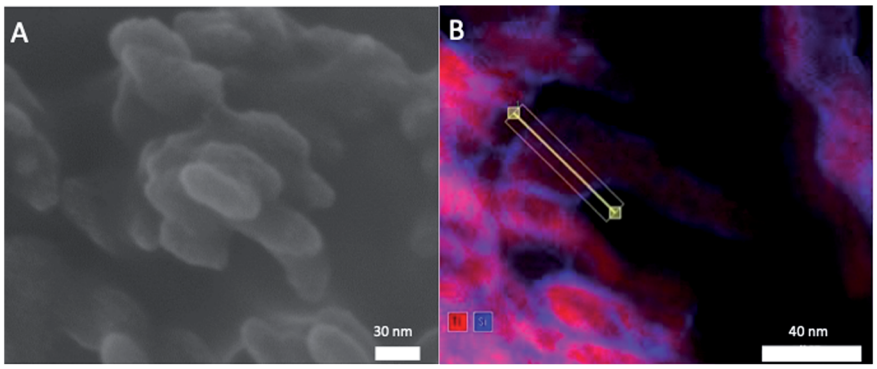

Fig. 2 (A) SEM image and (B) EDS elemental map overlay (Ti = red, Si = blue) of pristine T-AVO.

Si) generated by energy-dispersive X-ray spectroscopy (EDX) was used to determine a SiO_2 layer thickness of 3.6 ± 0.3 nm (Fig. 2B, $n = 12$ measurements).

To investigate the nature of the bonding between the TiO_2 core and the SiO_2 protective shell at the molecular level, ^{29}Si SSNMR was used to characterize the contributions of Q^4, Q^3, Q^2, and Si–O–Ti species. The ^{29}Si SPE MAS spectrum of pristine T-AVO (Fig. 3 inset) displays a large predominant contribution at −111 ppm, which corresponds to Q^4 Si tetrahedra within the silica (*i.e.* Si with 4 neighboring SiO groups). Lines downfield from this −111 ppm resonance are attributed to $Q^{<4}$ Si tetrahedra and Si–O–Ti species. Due to the long recycle delay (20 s), data acquisition took over 2.5 days with a limited number of scans, which yielded a rather poor signal-to-noise ratio (S/N) and prevented clear peak assignment. Therefore, data analysis was limited to line fitting the spectrum to obtain approximate proportions of "core" *vs.* "surface" Si species (*viz. ca.* 80% for Q^4 Si and 20% for Q^2, Q^3 and Ti-bound Si combined).

As opposed to ^{29}Si SPE MAS NMR, where the area of each ^{29}Si resonance in the spectra reflects the actual proportion of the corresponding Si species within the sample, only Si atoms that are relatively close to protons produce a measurable signal in a ^{1}H → ^{29}Si CP MAS experiment. In the present case, due to the absence of protons in the Q^4-structured part of the coating, ^{1}H → ^{29}Si CP MAS (hereafter simply referred to as ^{29}Si CP MAS) can be regarded as a surface sensitive/selective method.

The DNP-enhanced ^{29}Si CP MAS spectrum of pristine T-AVO is reported in Fig. 3. It displays a series of resonances (at −102.4 ppm, −90.6 ppm, and −82.6 ppm) as well as

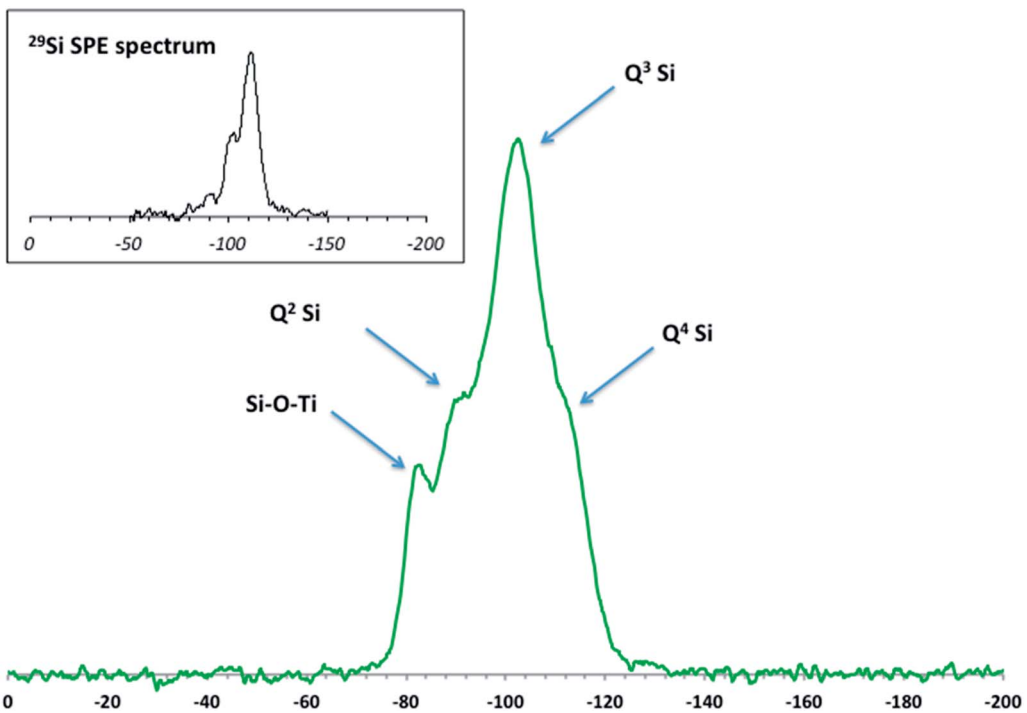

Fig. 3 DNP-enhanced ^{29}Si CP MAS solid-state NMR spectrum of the pristine T-AVO nanocomposite with spectral assignment. Inset: Single Pulse Excitation (SPE) ^{29}Si MAS solid-state NMR spectrum.

a poorly resolved shoulder at −111 ppm. The latter is due to Q^4 Si atoms and its relatively low intensity with respect to the other resonances results from the surface sensitive feature of CP MAS (*vide supra*). The resonances at −102.4 ppm and −90.6 ppm correspond to Q^3 and Q^2 Si species at the outer and inner surfaces of the coating. Moreover, the chemical shift of Q^1 Si (*i.e.* Si with 3 neighboring hydroxyl groups) is typically downfield from those due to Q^n (n: 2–4) Si sites. For example, in cement phases, the chemical shift of Q^1 Si (*i.e.* silica chain ends) is usually around −80 ppm.[27] However, in the present case, the occurrence of Q^1 Si within the silica is expected to be marginal at best. It is therefore unlikely that the significant contribution at −82.6 ppm observed here corresponds to isolated Q^1 Si. Instead, this resonance is within the range of chemical shifts previously described for Ti–O–Si bonds in titanosilicates.[28–30] The presence of these covalent bonds shows strong attachment of the silica coating to the underlying TiO_2 particle core. In addition, the strength of the signal at −82.6 ppm is the result of an efficient $^1H \rightarrow {}^{29}Si$ magnetization transfer, thus suggesting the presence of protons at the SiO_2–TiO_2 interface. However, from the present data, it is not possible to determine how this protonation is distributed between SiO_2 and TiO_2.

Quantitation of the Si at the inner surface of the coating that is covalently bound to the TiO_2 is also far from straightforward. In addition to other parameters, the signal strength significantly depends on the $^1H \rightarrow {}^{29}Si$ magnetization transfer. Here, where sites at the inner and outer surfaces of the SiO_2 shell need to be considered, the efficiency of this transfer is expected to be different. Indeed, in the case of "standard" CP MAS, the polarization of all ^1H is dependent on the applied external B_0 magnetic field, and thus the main factor affecting the transfer is the spatial distribution of protons within the sample. In a DNP-enhanced CP MAS experiment, improved sensitivity is achieved through hyperpolarization of the protons by using the unpaired electrons of paramagnetic species (*e.g.* radicals) that are added to the sample by impregnating it at room temperature with a radical-containing solution. As a result, the polarization of the ^1H spin system is no longer expected to be uniform throughout the sample, and polarization of protons at the interface between the core and the shell of a composite species is likely to be less effective than at the outer surface of this material, leading to a diminished magnetization transfer to the dilute spin, *viz.* ^{29}Si. Consequently, the intensity of the ^{29}Si NMR resonances due to the Si–O–Ti sites, as well as the Q^2 and Q^3 species at the inner surface of the coating shell, are presumably underestimated with respect to the actual proportions of these sites within the sample.

T-AVO nanocomposites aged in simulated fresh- and seawater lose protective SiO_2 shell

With sunscreen manufacturers recommending reapplication every 2 h, the use phase of the product by the consumer is rather short. In this context, the aging protocol selected for this work instead addressed the end-of-life phase of sunscreen TiO_2 UV filters released into aqueous environments (*e.g.* fresh- and seawater) during recreational activities. The 48 h agitation period simulates the initial dispersion of the material in the water column, while the subsequent 48 h settling period accounts for earlier determinations, in particular those using mesocosms, showing that a number of aged nanomaterials tend to accumulate in the benthic zone.[31–33] The simplified abiotic systems utilized here in no way perfectly represent a real ecosystem, but these simulated fresh- and seawater systems allowed for the assessment of a presumably minimum degradation scenario.

Silicon release from the T-AVO nanocomposite after 4 days (96 h) of aqueous aging is shown in Table 2. The most striking result is that nearly all (∼88–98%) of the protective SiO_2 layer around the TiO_2 UV filter was lost after a short 96 h period of aging in both the model continental and marine aqueous environments (fresh- and seawaters, respectively), whereas no significant Si release (∼1.5–2%) was observed for the sample aged in ultrapure water. There is no discernable difference in this phenomenon between the freshwater (commercial Cristaline® mineral water) and simulated seawater (Instant Ocean® mix) and either of the illumination regimes (daylight and dark). As a matter of fact, considering experimental uncertainties, the slightly lower release measured in the dark is not significantly different from the Si determination under artificial daylight. The same observation was made in ultrapure water where the presence or absence of daylight had no effect on the Si release. As a consequence, TiO_2 driven photo-reactivity is expected to be a minor factor (if any) in the Si release mechanisms. The quantitative loss of the protective SiO_2 coating in the model fresh-and seawaters during a relatively short aging period raises the question as to the mechanism(s) by which Si is removed from the TiO_2 core material. In a first approximation, the difference in Si release observed in the model fresh and seawater compared to the limited Si release in ultrapure water might indicate differences in the mechanism for these two situations. As opposed to ultrapure water, the observed rapid loss of the coating in the model waters suggests a non-gradual removal mechanism, *e.g.* flaking-off or delamination. To give insight as to the role that pH and ionic strength (IS) play in this mechanism, the T-AVO particles were also aged for 96 h in a lower ionic strength solution of 1 mM $NaHCO_3$ at a pH similar to that of the fresh- and seawaters, *i.e.* pH = 8. In these conditions, 19.0 ± 0.1% of the SiO_2 coating was degraded, compared to 92.4 ± 3.4 and 88.2 ± 2.3% in the fresh (IS = 5.8 mM) and seawaters (IS = 576 mM), respectively, thus suggesting an ionic strength accelerated release mechanism, as opposed to one driven by pH. From a safe(r)-by-design perspective applied to UV filters for use in sunscreens, knowledge of the Si release

Table 2 Percent degradation of T-AVO SiO_2 coating after 48 h aging and 48 h sedimentation in various aqueous solutions. Error represents variation between three separate aging experiments

Aqueous solution	Daylight	Dark
Ultrapure water	1.5 ± 0.1%	1.9 ± 0.5%
Freshwater	97.6 ± 8.8%	92.4 ± 3.4%
Seawater	94.3 ± 7.6%	88.2 ± 2.3%

mechanism is essential for the formulation of nanocomposites with a better aging/weathering resistance.

Examination of the Si speciation on the aged material provides better insight into how the protective SiO_2 layer is removed from the TiO_2 core. The DNP-enhanced ^{29}Si CP MAS spectra (Fig. 4) were normalized with respect to sample mass, number of scans, and DNP signal enhancement. As a comparison, the spectra obtained with "standard" CP MAS (*i.e.* without DNP and at room temperature) for the aged samples (Fig. 4 inset) were found to be unusable despite performing three times the number of scans. In this context, the added uncertainties regarding DNP NMR-based quantitation of sites in layered compounds are outweighed by the gain in S/N.

The speciation data obtained with NMR give a more detailed view of Si release than the ICP-based elemental analyses. Here, marked differences are observed between simulated fresh and seawater aging. Although, as mentioned above, quantitative exploitation of DNP-enhanced CP MAS data in the present study needs to be handled with care, there are obvious trends that can be validated beyond any uncertainty concerns. The main feature is the massive loss of signal (especially due to Q^4 Si) after aging in the model waters compared to pristine T-AVO. This is consistent with the ICP results, which show that virtually all of the SiO_2 was removed upon aging. However, there are differences between the aged materials. After aging in freshwater, the intensities of the Q^3 and Q^2 resonances are strongly reduced whereas the −82 ppm resonance (corresponding to the Si–O–Ti bonds) appears to be only slightly affected and becomes the predominant contribution in the ^{29}Si spectrum. In contrast, after aging in seawater, all resonances are strongly reduced. Keeping in mind all of the associated uncertainties, tentative semi-quantitative trends can be derived by line fitting the spectra. For the pristine T-AVO nanocomposite, the proportion of Si in Si–O–Ti bonds is ~6% of the whole ^{29}Si spectrum area, which translates to 12% of the Si sites on the inner surface of the coating, assuming that the surface areas of the inner and outer shells are not significantly different given the size of the TiO_2 core material and the thickness of the SiO_2 coating. For the freshwater-aged material, the proportion of Si–O–Ti bounds jumps to ~40%. Considering the low contributions of Q^2 and Q^3 Si, which also imply the removal of all associated Q^4 Si units, the CP MAS spectrum obtained for the freshwater-aged sample accounts for the entire Si remaining rather than just the "surface" species. In this context, the predominant Si–O–Ti proportion demonstrates: (i) a relative stability of these linkages since they are the last ones to be affected by aging, illustrating that at this point in the freshwater aging, nearly half of the remaining Si on the nanocomposite is associated with Ti (ii) Si removal progresses from the outside shell inwards, which excludes the possibility of a delamination process. The observed Si speciation is instead consistent with Si removal by dissolution.

After aging in seawater, even further SiO_2 layer degradation was observed compared to the freshwater conditions. Indeed, a rough line fitting analysis shows a decrease of ~66% of the detected Si compared to the freshwater-aged sample. Again,

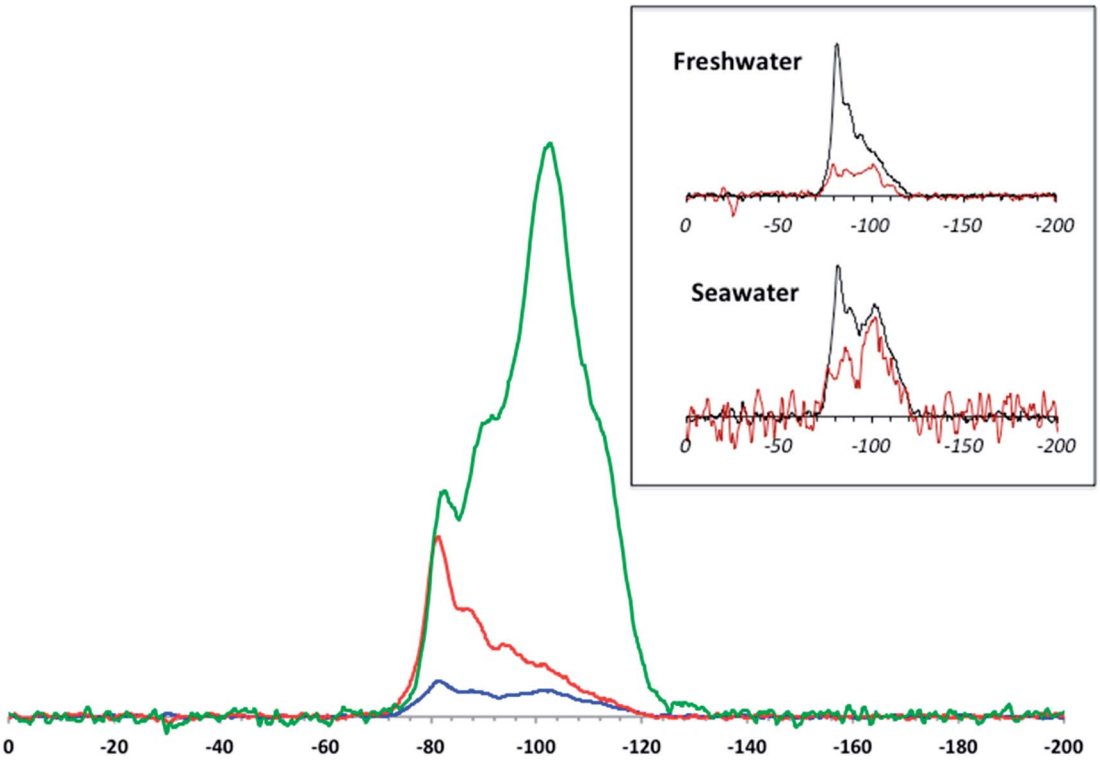

Fig. 4 Normalized DNP-enhanced ^{29}Si CP MAS solid-state NMR spectra of the pristine and aged T-AVO nanocomposite (green: pristine material; red: freshwater aged; blue: seawater aged). Inset: comparison between the DNP-enhanced ^{29}Si CP MAS spectra (black traces) and the "standard" ^{29}Si CP MAS spectra (brown traces, magnified 4 times) for the T-AVO nanocomposite aged in freshwater and seawater.

assuming that the DNP-enhanced CP MAS signal accounts for all the Si remaining on the aged nanocomposite, this shows a quasi-complete depletion of the protective layer at the surface of the TiO_2 surface, including the presumably more stable Si–O–Ti species.

There is a clear progression of the Si speciation according to the ionic strength: freshwater causes quantitative dissolution of silica but preserves Si–O–Ti bonds, whereas seawater (with its higher salt content) affects all Si sites. Indeed, the solubility of amorphous silica has received a great deal of attention and its dependence on the ionic strength of the medium has already been demonstrated.[34] The general trend observed in the present study shows an enhanced solubility with increasing salt content. Nevertheless, the difference in dissolution rates differs from what is usually described in previous studies. Previous findings revealed an acceleration in the dissolution rate by as much as 20× when the ionic strength was raised to 50 mM.[34] In the present case, an ionic strength 10× lower (simulated freshwater) resulted in an even higher increase in the dissolution rate, *viz.* a factor of ∼40× (at least) compared to ultrapure water. However, the present data do not provide any leads regarding the mechanism behind these apparently faster kinetics.

Implications regarding safe(r)-by-design mineral UV filters

To determine the stability and/or persistence of a protective shell, it is essential to have access to reliable speciation data to help identify the mechanisms controlling the evolution of this layer during aging. From a technical point of view, DNP NMR proved to be an indispensable tool in this study by showing that the SiO_2 coating is removed from the outside inwards, most likely by simple dissolution. Furthermore, DNP NMR provided an analytical sensitivity superior to ICP determinations, which are generally considered to be the reference that all other elemental analysis methods are compared against.

In the present case, it was found that under environmentally relevant aging conditions, the SiO_2 protective coating around the TiO_2 filter has a lifetime of less than 4 days in simulated fresh- and seawater. While substantial Si–O–Ti binding is still detected after freshwater aging, Si dissolution in the simulated seawater (with a 10× higher ionic strength) leaves very little of the initial Si at the surface of the TiO_2 core particle (Fig. 4). It can be hypothesized that a more prolonged aging in freshwater would also lead to a comparable removal of the SiO_2 coating. Furthermore, it can be assumed that the nanocomposite becomes photoreactive/phototoxic with aging as a result of this loss of the SiO_2 protective coating. As such, detailed quantitation of the reactive oxygen species generated from the aged T-AVO by-products is currently under investigation. The SiO_2 coating protects the consumer from TiO_2 driven photoreactivity, however the present data show that upon release into the aqueous environment this protective coating disappears, exposing the bare TiO_2 core and possibly resulting in detrimental environmental effects against several types of biota, including coral reefs.[14–19] Indeed, although the nanocomposite is included within an organic formulation in the final sunscreen product, the organic matrix has a limited lifetime and in some cases may detach from the mineral composite after periods of as short as 24 h,[21,35] exposing the SiO_2 and allowing dissolution to proceed from that point on.

As a matter of fact, previous findings have shown that the nanocomposites in sunscreens are released to the aquatic environment in a non-dispersed form, and increasing the ionic strength results in even further aggregation of the residue.[35] This aggregation state might become an aggravating factor in terms of environmental effects. Indeed, the aggregates precipitate and/or attach to immersed solid structures, including reefs. The potential increased amount of pollutants in the vicinity of (or attached to) fragile structures is likely to have accentuated detrimental effects once the organic matrix and the protective layer are weathered.

The T-AVO nanocomposite examined here can/needs to be improved for a better environmental sustainability. Attachment of the SiO_2 layer to the UV filter is not a concern since we estimated that at least 12% of surface Si atoms are engaged in covalent bonds with the TiO_2 core. However, the resistance of the coating to even mild aging conditions is poor. Preventing the degradation of the coating, and consequently preventing TiO_2 phototoxicity, can be achieved by either isolating the SiO_2 layer from water with a water-resistant shell, or by using less soluble or insoluble Si polymorphs. Additional work still needs to be done in providing the market with environmentally safe and sustainable sunscreens that also satisfy consumer needs and public health requirements.

Conflicts of interest

The authors declare that there is no conflict of interest to report.

Acknowledgements

This work has received funding from the Excellence Initiative of Aix-Marseille University – A*MIDEX, a French "Investissements d'Avenir" program, through its associated Labex SERENADE project. This work is also a contribution to the OSU-Institut Pythéas. The authors thank Dr Daniel Borschneck of the CEREGE for assistance with XRD analysis. The authors also acknowledge the CNRS for the funding of the IRP iNOVE as well as the funding of the PICS no. 08322 SODA Light.

References

1 R. B. Raffa, J. V. Pergolizzi, R. Taylor, J. M. Kitzen and N. R. Grp, Sunscreen bans: coral reefs and skin cancer, *J. Clin. Pharm. Ther.*, 2019, **44**, 134–139.
2 S. L. Schneider and H. W. Lim, Review of environmental effects of oxybenzone and other sunscreen active ingredients, *J. Am. Acad. Dermatol.*, 2019, **80**, 266–271.
3 R. Danovaro, L. Bongiorni, C. Corinaldesi, D. Giovannelli, E. Damiani, P. Astolfi, L. Greci and A. Pusceddu, Sunscreens cause coral bleaching by promoting viral infections, *Environ. Health Perspect.*, 2008, **116**, 441–447.

4 M. E. Balmer, H. R. Buser, M. D. Muller and T. Poiger, Occurrence of some organic UV filters in wastewater, in surface waters, and in fish from Swiss lakes, *Environ. Sci. Technol.*, 2005, **39**, 953–962.

5 J. C. DiNardo and C. A. Downs, Dermatological and environmental toxicological impact of the sunscreen ingredient oxybenzone/benzophenone-3, *J. Cosmet. Dermatol.*, 2018, **17**, 15–19.

6 P. Gago-Ferrero, M. Silvia Diaz-Cruz and D. Barcelo, An overview of UV-absorbing compounds (organic UV filters) in aquatic biota, *Anal. Bioanal. Chem.*, 2012, **404**, 2597–2610.

7 K. H. Langford, M. J. Reid, E. Fjeld, S. Oxnevad and K. V. Thomas, Environmental occurrence and risk of organic UV filters and stabilizers in multiple matrices in Norway, *Environ. Int.*, 2015, **80**, 1–7.

8 P. Filipe, J. N. Silva, R. Silva, J. L. C. de Castro, M. M. Gomes, L. C. Alves, R. Santus and T. Pinheiro, Stratum Corneum is an Effective Barrier to TiO_2 and ZnO Nanoparticle Percutaneous Absorption, *Skin Pharmacol. Physiol.*, 2009, **22**, 266–275.

9 E. Kimura, Y. Kawano, H. Todo, Y. Ikarashi and K. Sugibayashi, Measurement of Skin Permeation/Penetration of Nanoparticles for Their Safety Evaluation, *Biol. Pharm. Bull.*, 2012, **35**, 1476–1486.

10 P. J. Lu, S. C. Huang, Y. P. Chen, L. C. Chiueh and D. Y. C. Shih, Analysis of titanium dioxide and zinc oxide nanoparticles in cosmetics, *J. Food Drug Anal.*, 2015, **23**, 587–594.

11 L. S. Silva and M. Monteiro, Safety Evaluation of the Nanoparticles of Titanium Dioxide and Zinc Oxide in Antissolar Formulations, *Rev. Virtual Quim.*, 2016, **8**, 1963–1977.

12 E. B. Manaia, R. C. K. Kaminski, M. A. Correa and L. A. Chiavacci, Inorganic UV filters, *Braz. J. Pharm. Sci.*, 2013, **49**, 201–209.

13 N. Serpone, D. Dondi and A. Albini, Inorganic and organic UV filters: their role and efficacy in sunscreens and suncare product, *Inorg. Chim. Acta*, 2007, **360**, 794–802.

14 L. K. Adams, D. Y. Lyon and P. J. J. Alvarez, Comparative eco-toxicity of nanoscale TiO_2, SiO_2, and ZnO water suspensions, *Water Res.*, 2006, **40**, 3527–3532.

15 V. Aruoja, H. C. Dubourguier, K. Kasemets and A. Kahru, Toxicity of nanoparticles of CuO, ZnO and TiO_2 to microalgae Pseudokirchneriella subcapitata, *Sci. Total Environ.*, 2009, **407**, 1461–1468.

16 S. Schiavo, M. Oliviero, A. Philippe and S. Manzo, Nanoparticles based sunscreens provoke adverse effects on marine microalgae Dunaliella tertiolecta, *Environ. Sci.: Nano*, 2018, **5**, 3011–3022.

17 Z. Wang, B. Xia, B. Chen, X. Sun, L. Zhu, J. Zhao, P. Du and B. Xing, Trophic transfer of TiO_2 nanoparticles from marine microalga (Nitzschia closterium) to scallop (Chlamys farreri) and related toxicity, *Environ. Sci.: Nano*, 2017, **4**, 415–424.

18 C. Corinaldesi, F. Marcellini, E. Nepote, E. Damiani and R. Danovaro, Impact of inorganic UV filters contained in sunscreen products on tropical stony corals (Acropora spp.), *Sci. Total Environ.*, 2018, **637**, 1279–1285.

19 J. P. Fel, C. Lacherez, A. Bensetra, S. Mezzache, E. Beraud, M. Leonard, D. Allemand and C. Ferrier-Pages, Photochemical response of the scleractinian coral Stylophora pistillata to some sunscreen ingredients, *Coral Reefs*, 2019, **38**, 109–122.

20 Y. Li, W. Zhang, J. F. Niu and Y. S. Chen, Mechanism of Photogenerated Reactive Oxygen Species and Correlation with the Antibacterial Properties of Engineered Metal-Oxide Nanoparticles, *ACS Nano*, 2012, **6**, 5164–5173.

21 M. Auffan, M. Pedeutour, J. Rose, A. Masion, F. Ziarelli, D. Borschneck, C. Chaneac, C. Botta, P. Chaurand, J. Labille and J. Y. Bottero, Structural Degradation at the Surface of a TiO_2-Based Nanomaterial Used in Cosmetics, *Environ. Sci. Technol.*, 2010, **44**, 2689–2694.

22 S. R. Al-Abed, J. Virkutyte, J. N. R. Ortenzio, R. M. McCarrick, L. L. Degn, R. Zucker, N. H. Coates, K. Childs, H. Ma, S. Diamond, K. Dreher and W. K. Boyes, Environmental aging alters $Al(OH)_3$ coating of TiO_2 nanoparticles enhancing their photocatalytic and phototoxic activities, *Environ. Sci.: Nano*, 2016, **3**, 593–601.

23 J. Virkutyte, S. R. Al-Abed and D. D. Dionysiou, Depletion of the protective aluminum hydroxide coating in TiO_2-based sunscreens by swimming pool water ingredients, *Chem. Eng. J.*, 2012, **191**, 95–103.

24 A. S. L. Thankamony, J. J. Wittmann, M. Kaushik and B. Corzilius, Dynamic nuclear polarization for sensitivity enhancement in modern solid-state NMR, *Prog. Nucl. Magn. Reson. Spectrosc.*, 2017, **102**, 120–195.

25 A. Lesage, M. Lelli, D. Gajan, M. A. Caporini, V. Vitzthum, P. Mieville, J. Alauzun, A. Roussey, C. Thieuleux, A. Mehdi, G. Bodenhausen, C. Coperet and L. Emsley, Surface Enhanced NMR Spectroscopy by Dynamic Nuclear Polarization, *J. Am. Chem. Soc.*, 2010, **132**, 15459–15461.

26 C. Sauvee, M. Rosay, G. Casano, F. Aussenac, R. T. Weber, O. Ouari and P. Tordo, Highly Efficient, Water-Soluble Polarizing Agents for Dynamic Nuclear Polarization at High Frequency, *Angew. Chem., Int. Ed.*, 2013, **52**, 10858–10861.

27 F. Meducin, B. Bresson, N. Lequeux, M. N. de Noirfontaine and H. Zanni, Calcium silicate hydrates investigated by solid-state high resolution H-1 and Si-29 nuclear magnetic resonance, *Cem. Concr. Res.*, 2007, **37**, 631–638.

28 M. L. Balmer, B. C. Bunker, L. Q. Wang, C. H. F. Peden and Y. L. Su, Solid-state Si-29 MAS NMR study of titanosilicates, *J. Phys. Chem. B*, 1997, **101**, 9170–9179.

29 B. R. Cherry, M. Nyman and T. M. Alam, Investigation of cation environment and framework changes in silicotitanate exchange materials using solid-state Na-23, Si-29 and Cs-133 MAS NMR, *J. Solid State Chem.*, 2004, **177**, 2079–2093.

30 J. Xu, B. E. G. Lucier, Z. Lin, A. Sutrisno, V. V. Terskikh and Y. Huang, New Insights into the Short-Range Structures of Microporous Titanosilicates As Revealed by Ti-47/49, Na-23, K-39, and Si-29 Solid-State NMR Spectroscopy, *J. Phys. Chem. C*, 2014, **118**, 27353–27365.

31 M. Auffan, M. Tella, C. Santaella, L. Brousset, C. Pailles, M. Barakat, B. Espinasse, E. Artells, J. Issartel, A. Masion,

J. Rose, M. R. Wiesner, W. Achouak, A. Thiery and J. Y. Bottero, An adaptable mesocosm platform for performing integrated assessments of nanomaterial risk in complex environmental systems, *Sci. Rep.*, 2014, **4**, 5608.

32 M. Tella, M. Auffan, L. Brousset, J. Issartel, I. Kieffer, C. Pailles, E. Morel, C. Santaella, B. Angeletti, E. Artells, J. Rose, A. Thiery and J. Y. Bottero, Transfer, Transformation, and Impacts of Ceria Nanomaterials in Aquatic Mesocosms Simulating a Pond Ecosystem, *Environ. Sci. Technol.*, 2014, **48**, 9004–9013.

33 M. Tella, M. Auffan, L. Brousset, E. Morel, O. Proux, C. Chaneac, B. Angeletti, C. Pailles, E. Artells, C. Santaella, J. Rose, A. Thiery and J. Y. Bottero, Chronic dosing of a simulated pond ecosystem in indoor aquatic mesocosms: fate and transport of CeO_2 nanoparticles, *Environ. Sci.: Nano*, 2015, **2**, 653–663.

34 J. P. Icenhower and P. M. Dove, The dissolution kinetics of amorphous silica into sodium chloride solutions: effects of temperature and ionic strength, *Geochim. Cosmochim. Acta*, 2000, **64**, 4193–4203.

35 C. Botta, J. Labille, M. Auffan, D. Borschneck, H. Miche, M. Cabie, A. Masion, J. Rose and J. Y. Bottero, TiO_2-based nanoparticles released in water from commercialized sunscreens in a life-cycle perspective: structures and quantities, *Environ. Pollut.*, 2011, **159**, 1543–1548.

